

This PDF has been sent from one of the University of Delaware's partner libraries through Interlibrary Loan. It will be in your account for **30** days. After 30 days, the PDF will be permanently deleted.

If you received the wrong item, or if there are any other problems with the PDF (such as missing pages or unclear images), **please contact the**Interlibrary Loan Office. We will ask the supplier for a corrected copy.

Interlibrary Loan Office AskILL@udel.libanswers.com

# NOTICE: WARNING CONCERNING COPYRIGHT RESTRICTIONS

The copyright law of the United States (Title 17, United States Code) governs the making of photocopies or other reproductions of copyrighted material.

Under certain conditions specified in the law, libraries and archives are authorized to furnish a photocopy or other reproduction. One of these specified conditions is that the photocopy or reproduction is not to be "used for any purpose other than private study, scholarship, or research." If a user makes a request for, or later uses, a photocopy or reproduction in excess of "fair use," that user may be liable for copyright infringement.

This institution reserves the right to refuse to accept a copying order if, in its judgment, fulfillment of the order would involve violation of copyright law.

Articles received through Interlibrary Loan may not be redistributed.



FISEVIER

Contents lists available at ScienceDirect

# Journal of Analytical and Applied Pyrolysis

journal homepage: www.elsevier.com/locate/jaap





# Production and characterization of a high value-added seaweed-derived biochar: Optimization of pyrolysis conditions and evaluation for sediment treatment

Chang-Mao Hung <sup>a</sup>, Chin-Pao Huang <sup>b</sup>, Jia-Wei Cheng <sup>a</sup>, Chiu-Wen Chen <sup>a,\*</sup>, Cheng-Di Dong <sup>a,\*</sup>

- <sup>a</sup> Department of Marine Environmental Engineering, National Kaohsiung University of Science and Technology, Kaohsiung City, Taiwan
- b Department of Civil and Environmental Engineering, University of Delaware, Newark, USA

#### ARTICLE INFO

Keywords: Seaweed-derived biochar Peroxymonosulfate PAHs Sargassum duplicatum

#### ABSTRACT

Biochar is a promising material for removing contaminants in sediments. Here, thermal carbonization was carried out to convert a brown seaweed ( $Sargassum\ duplicatum$ ) into a high value-added biochar, which was used to activate peroxymonosulfate (PMS) in environmental remediation applications. XRD, FTIR, XPS, C-H-O elemental analysis, and SEM results showed that pyrolysis temperature ( $300-700\,^{\circ}$ C) had a significant influence on the crystal structure, surface functional groups, chemical composition, morphology and porosity of the brown seaweed-derived biochar (BSB). When the biochar samples were tested with PMS for removing polycyclic aromatic hydrocarbons (PAHs, a type of carcinogenic and refractory organic compounds) from marine sediments, pyrolysis temperature also showed crucial effects, and the sample pyrolyzed at 700 °C was most effective for the oxidative removal of PAHs. Under the optimum conditions (pH<sub>0</sub> = 3.0, [BSB] = 3.0 g/L, [PMS]: $\sum$ [PAH] = 1:1, and 10 h reaction time), 77 % of PAHs was eliminated with the maximum degradation rates of 87, 79, 67, 55, and 10 or the 6-ring, 5-ring, 4-ring, 3-ring, and 2-ring PAHs, respectively. EPR results confirmed that SO<sub>4</sub> and HO• radicals play main roles in the catalytic degradation of PAHs. Based on these results, the sustainably produced BSB has good prospects for the seaweed bioeconomy and remediating organics-contaminated sediments.

#### 1. Introduction

The presence of carcinogenic and refractory organic compounds, specifically, polycyclic aromatic hydrocarbons (PAHs), in estuarine and coastal sediments becomes a severe pollution problem globally, which endangers both ecosystems and human health [1]. PAHs were priority pollutants listed by US Environmental Protection Agency due to their hydrophobic, lipophilic, persistent, ecotoxic, mutagenic, and strongly persistent nature [2]. Therefore, there is an urgent need to eliminate PAHs from contaminated sediments [3].

Several approaches have been advanced to remediate refractory aromatic organic contaminants in marine sediments [4–16]. Due to strong oxidation ability and benign characteristics, peroxygens such as peroxydisulfate (PDS,  $S_2O_8^{2-}$ ) and peroxymonosulfate (PMS,  $HSO_5$ ) have been reported to effectively degrade a wide range of pollutants to small organic acid molecules through hydrogen and electron abstraction/addition [17–20]. There have much interest on advanced oxidation based on sulfate and hydroxyl radicals ( $SO_4^{\bullet-}$  +  $e^-$  =  $SO_4^{2-}$ ;  $E^0$  = 3.1 V vs

NHE;  $HO \cdot + e^- = OH^-$ ;  $E^0 = 2.7 \text{ V}$  vs NHE) using PMS. With respect to Fenton reagent, PMS-based peroxygen systems have several attributes including high stability over wide pH range, mild reaction conditions, high treatment efficiency, and less toxic products [21].

Further, carbon-rich aquatic biomass could be converted readily to value-added biochar by carbonization under oxygen-limited environment. Engineered biochar has found wide applications in environmental remediation, sustainable agriculture, and energy production owing to its highly porous framework, moisture retention, and pH buffer intensity [22], in addition to high specific surface area, and abundant oxygen functional species of high metal adsorption capacity [23]. Feedstock characteristics and pyrolysis temperature are among the most significant factors affecting the physical-chemical properties of biocahrs. For examples, Wan Mahari et al. (2020) reported that highly porous palm kernel shell biochar shortened the formation, growth and full colonization of mycelium, which significantly improved mushroom yield [22]. Ren et al. (2021) demonstrated that heavy metal adsorption capacity incurred in biochars significantly improved tobacco production [23]. Accordingly,

E-mail addresses: cwchen@nkust.edu.tw (C.-W. Chen), cddong@nkust.edu.tw (C.-D. Dong).

<sup>\*</sup> Corresponding authors.

there are numeral research activities to utilize biomass-derived carbon supported with non-metals or transition metals as PMS activators to generate SO<sub>4</sub> - radical [24]. Zhao et al. (2018) studied the discoloration of methylene blue (MB) in water by PMS activated with seaweed-derived multifunctional nitrogen/cobalt-codoped carbonaceous beads (MCB) and reported efficient reduction of MB brought by highly oxidizing reactive oxygen species such as SO<sub>4</sub>• and HO• in the MCB/PMS system [25]. Ye et al. (2020) utilized high-performance graphitization and nitrogen doping technique to prepare highly reactive biochar catalysts, metal free with agricultural waste fibers, for PMS activation in the degradation of tetracycline (TC) [21]. In the process, oxygen reactive species such as SO<sub>4</sub>•-, HO• and <sup>1</sup>O<sub>2</sub> were being continuously generated from the ketone functional group, graphitic nitrogen, and surface defects on the carbon framework, typical advanced oxidation reactions based on sulfate radical. Xie et al. (2020) prepared a nitrogen-doped biochar nanosheet via molten salt pyrolysis process using Candida utilis biomass as PMS activator and reported 100 % bisphenol A (BPA) removal in 6 min [26]. The lamellar structure, increase in defects, and high surface graphitic N and pyridinic-N in the biochar significantly enhanced its catalytic reactivity. Yang et al. (2019) investigated the degradation of acetaminophen (ACE) by PMS in the presence of Co-impregnated lignin biochar (CoIB)-activator, and demonstrated that SO4, and HO• enabled the complete removal of ACE [27]. Guo et al. (2020) demonstrated the activation of PMS by corn straw biochar and reported effective treatment of benzo[a]pyrene (BaP)-polluted soils [28].

In summary, value-added carbonaceous materials derived from seaweed specifically may be cost-effective and eco-friendly heterogeneous catalyst for the *in-situ* or *ex-situ* remediation of PAH-contaminated sediments [29]. We have previously demonstrated that red seaweed-derived biochar could promote the oxidation of 4-nonylphenol in impaired aquatic sediments [13]. In the present study, we further converted a brown seaweed into a carbonaceous solid matrix through thermal carbonization. The produced biochar energized PMS for producing reactive oxygen species to oxidize PAHs in aquatic sediments. To the best of our knowledge, there has no report on the use of brown seaweed biochar (BSB) for the PMS-mediated oxidation of PAHs.

During the production of biochar, the pyrolysis temperature affects not only the aromaticity and aromatic condensation but also the structural characteristics and morphology of the product [30]. Therefore, the main goals of this study were: (1) to explore the influence of carbonization temperature (300–700 °C) on the crystal structure, surface functional groups, surface elemental composition, morphology, and porosity of BSB; (2) to investigate the effects of various process parameters (i.e. pyrolysis temperature, PMS and BSB catalyst dosages, and initial pH) on the degradation of PAHs in the sediment; and (3) to establish mechanisms of the radical-mediated process and reveal the crucial role of BSB in the activation of PMS for PAHs degradation in contaminated sediments.

#### 2. Experimental

#### 2.1. Chemicals

Oxone® (2KHSO<sub>5</sub>•KHSO<sub>4</sub>•K<sub>2</sub>SO<sub>4</sub>) and 5,5-dimethyl-1-pyrroline Noxide (DMPO, 98.0 %) were purchased from Sigma-Aldrich Co., Ltd. (St. Louis, USA). Acetone, methanol, and *n*-hexane were procured from Merck (Darmstadt, Germany). Standard of 16 PAH chemicals (80 mg/L), internal PAH standard (4000 mg/L), and standard PAH surrogate (2000 mg/L) were provided by AccuStandard Chem. Co. (New Haven, CT, USA). All chemicals were belonged to analytical grade and used directly as received. All working solutions were prepared with deionized (DI) water. The 16 standard PAHs were: naphthalene (NA), acenaphthylene (ACY), acenaphthene (ACE), fluorene (FL), phenanthrene (PH), anthracene (AN), fluoranthene (FLU), pyrene (PY), benzo[a]anthracene (BaA), chrysene (CH), benzo[b]fluoranthene (BbF), benzo[k]fluoranthene (BkF), benzo[a]pyrene (BaP), indeno[1,2,3-cd]pyrene (IP),

dibenzo[a,h]anthracene (DA), and benzo[g,h,i]pervlene (BP).

#### 2.2. Collection of sediment samples

Sediments were collected, using n-hexane pre-washed glass bottles, at the top 0–15 cm in Kaohsiung Harbor ( $22^{\circ}32.420'$  N  $120^{\circ}20.638'$ E), Taiwan. The bottles were sealed right away and frozen while being brought back to the laboratory. All sediment samples were dried under ambient conditions for seven days, then blended thoroughly and ground to powders. Passed the powders first through a 2-mm, a 0.5-mm ASTM sieve, then ground the fines again with a mortar before freeze-drying for 72 h.

#### 2.3. Preparation of biochar from seaweed

Pristine seaweed (*Sargassum duplicatum*) was contributed by Po-Wu Biotechnology Co., Ltd. (Pintung, Taiwan). Washed the seaweed thoroughly in ultrapure water several times to get rid of dirt, and then airdried at 105 °C for 48 h. The dried seaweed was then carbonized in a single step using a furnace (NBD-01200, Nobody Materials Science and Technology Co., Ltd., Henan, China) under CO $_2$  environment at 300–700 °C (heating rate: 10 °C/min) for 180 min. The final product was ground by a cutting mill and identified as BSBX; X stands for the temperature of pyrolysis.

#### 2.4. Characterization of prepared BSB

A Diano-8536 diffractometer with Cu Kα radiation source was employed to obtain X-ray diffraction (XRD) spectra. A FT-700 spectrometer (Horiba, Japan) was used to obtain Fourier-transform infrared (FTIR) spectra, based on 32 scans with a 4-cm<sup>-1</sup> resolution. X-ray photoelectron spectroscopy (XPS; AXIS Ultra DLD, Kratos Analytical Ltd., Manchester, UK) analysis provided the state of key surface elemental species of BSB. The C, H, and O content were determined with an elemental analyzer (Vario EL III, Hanau, Germany). The morphology and porosity of BSB were characterized by scanning electron microscope (SEM) (Quanta 200 FEG, FEI Company, Brno-Černovice, Czech Republic). Electron paramagnetic resonance spectroscopy (EPR; EMXnano, Bruker, Germany) gave the identity and quantity of SO<sub>4</sub>• and HO• radicals, employing DMPO (0.1 M) as spin-trappant. The radical concentration of SO<sub>4</sub>• and HO• were established after background noise correction with respect to DMPO-SO<sub>4</sub>• and DMPO− HO• peaks, respectively.

#### 2.5. PAH degradation experiments

Experiment for PAH oxidative degradation was conducted with 40-mL borosilicate glass vials, containing 1 g sediment powder, 25 mL PMS at ( $\Sigma$ [PAH]:[PMS] from 1:1 to 1:100. The temperature was 25 °C. The bottles were continually shaken (200 rpm) in constant-temperature water bath and shaker (SB-9D, Hipoint Corporation, Kaohsiung, Taiwan). To study the effect of BSB dosage on PAH degradation, given amount of BSB was added to the solution to final concentration of 1.0–7.0 g/L. All experiments and controls were run in triplicates. At predetermined time, the oxidation reaction was stopped by methanol. Afterward, a mixed solvent (acetone:n-hexane = 1:1 v/v) was added, and the mixture was sonicated to extract the residual PAHs.

## 2.6. PAH analyses

Concentrations of the 16 PAHs in the liquid extract were determined by gas chromatograph (Model 6890; Agilent Technologies, CA, USA) supported by mass-selective detector (Model 5975; Agilent Technologies, CA, USA) in ion monitor mode. The temperature were 300, 280, and 230 °C in the split/splitless injector (Model 7683B, 1-min splitless time, 60-mL/min flow rate), transfer line, and ion source, respectively.

PAHs were separated with capillary column (HP-5MS, Hewlett-Packard, Palo Alto, CA, USA), 30 m long, 0.25 mm inner in diameter, and 0.25  $\mu m$  in film thickness. Helium was the carrier gas at one mL per min flow rate. The column temperature for PAH separation was: initially 40 °C for 1 min, then 120 °C at 25 °C/min, 160 °C at 10 °C/min, and finally 300 °C at 5 °C/min. Acceptable determination coefficient set at  $r^2=0.98$  for all calibrations.

#### 3. Results and discussion

#### 3.1. The surface properties of BSB

Fig. 1a shows the XRD spectrum of BSB. Results showed strong and narrow XRD peaks, which demonstrate the high-degree crystallinity of the biochar. The diffraction peaks at  $2\theta$   $23.7^{\circ}$  and  $43.9^{\circ}$  could be assigned to the (002) and (100) planes of amorphous and crystalline carbons, respectively [30]. The BSB had a peak at 20 26.6°, typical of crystalline carbon, which was characteristic of the (111) plane. The diffraction peaks were intensified when the temperature was increased from 300 to 700 °C, suggesting ordering of the BSB surface when the carbonaceous material was gradually transformed into graphite under high temperature [31]. Peaks at  $2\theta$  31.6°, 36.3°, 47.3°, and 64.1°, signifying the presence of CaO, belonged to the facets of (111), (200), and (222) [13]. The peaks at  $20\ 23.0^{\circ}$ ,  $29.4^{\circ}$ ,  $35.9^{\circ}$ ,  $43.2^{\circ}$ ,  $47.5^{\circ}$ ,  $48.5^{\circ}$ ,  $57.4^{\circ}$ ,  $60.6^{\circ}$ , and  $64.6^{\circ}$  represented the CaCO<sub>3</sub> facets of (012), (104), (110), (202), (018), (116), (122), (119), and (300), respectively [32]. All of above peaks were observed under higher pyrolysis temperature. In BSB700 (pyrolyzed at 700 °C), the intense CaO and CaCO3 peaks in addition to strong signals of graphite-like structures, which indicated the formation of CaCO<sub>3</sub> when the seaweed was carbonized with CO<sub>2</sub>. Recently, Yang et al. (2019) reported that pyrolysis in CO2 gas noticeably increased the porosity of biochars [27]. Furthermore, Hung et al. (2020) suggested that reaction between  $CO_2$  and CaO or  $Ca(OH)_2$  formed  $CaCO_3$ , which acted as an activation agent to produce favorable porous structures in the graphitic carbon matrix [13].

Fig. 1b show the FTIR spectra of surface functional groups of the BSB samples produced at different pyrolysis temperatures. The spectral band at around ~3400 cm<sup>-1</sup> was attributed to the surface –OH groups with hydrogen bonding to interlayer water molecules. The peaks at 1470, 689, and 907 cm<sup>-1</sup> represented the asymmetric stretching modes of Ca-O bonds [33]. Moreover, signals at 873, 1040, 1065, 1155, 1435, 1623, and 2848 cm<sup>-1</sup> were corresponding to the C-H, C-O-C, C-OH, C-H, –COO, C=C/C=O, and C–H bond stretching vibrations from the aromatic ring, individually [31,34]. The intensity of four peaks (C-O-C, -COO, C=C, and C=O) increased with rising carbonization temperature, which indicated aromatic carbon compounds were central to the biochar structure. The enhanced C=O groups probably were converted from the unstable C-O groups [30]. Furthermore, the C=O groups fostered the self-dissociation of PMS to yield <sup>1</sup>O<sub>2</sub> by electron transport between the pollutant molecules and the graphitized structures [35]. In contrast, these surface functional groups on BSB were weakened when the seaweed was pyrolyzed at 300-500 °C, due to combustion reactions of organic and volatile components of raw materials under pyrolysis. The above results indicated that surface functional groups played key roles during carbonization of brown seaweed for the production of BSB. Results of FTIR analysis further affirmed the success in depositing CaO phase onto the porous carbon structure via the Ca-O-C linkage. Previous studies have suggested that the Ca-O-C bond increased the chemical integrity of composite Ca-based catalysts and minimized loss of calcium ions [33]. XRD and FTIR data clearly revealed the existence of calcium oxide and calcium carbonate on BSB.

Fig. 1c shows the XPS survey data of BSB, which can be divided into

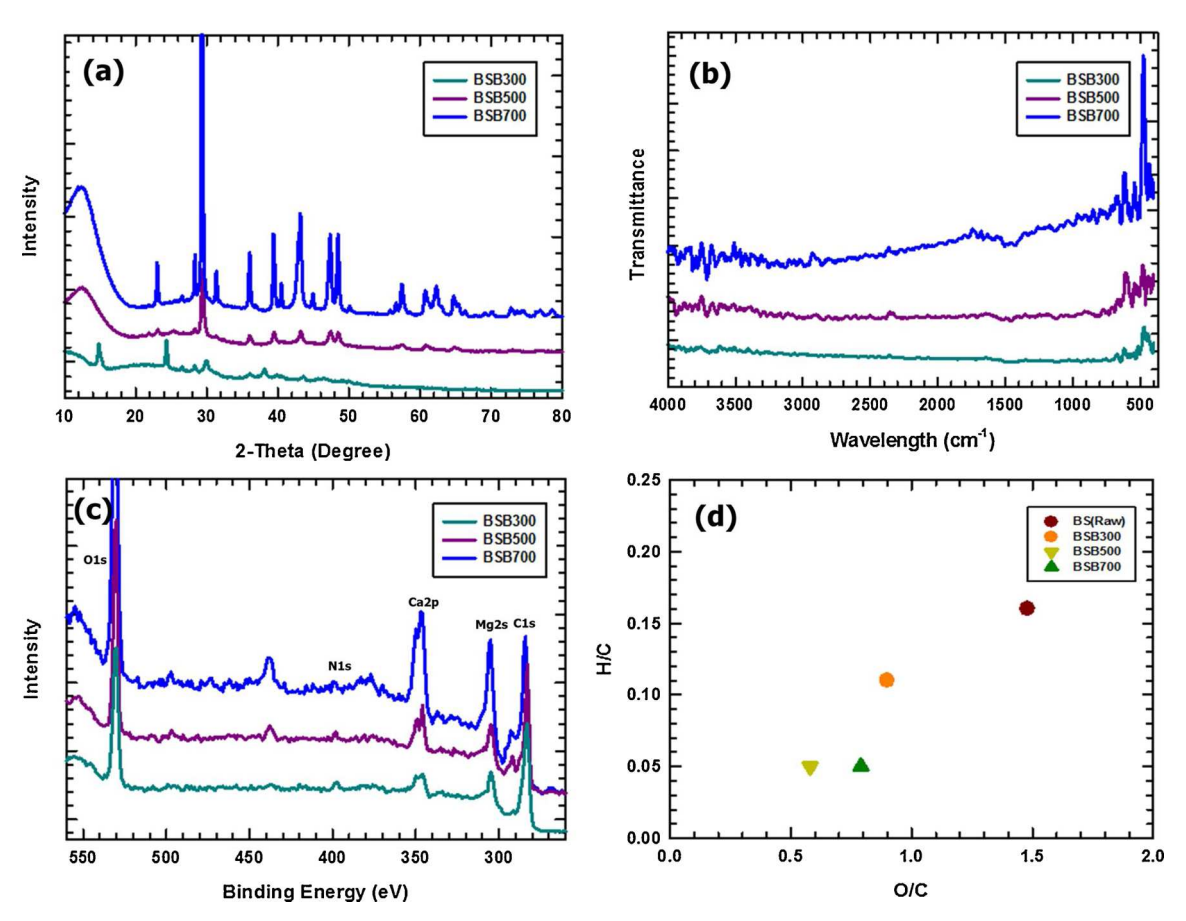


Fig. 1. Characterization of BSB. (a) XRD pattern, (b) FTIR, (c) XPS spectra, and (d) Van Krevelen plot.

five main peaks ascribed to O1s, N1s, Ca2p, Mg2s, and C1s, respectively. The existence of O, N, Ca, Mg, and C elements agreed well with the XRD and FTIR results. At higher carbonization temperature, the content of C decreased whereas that of Ca, Mg, and O increased. Specifically, the C1s peak was significantly weaker and that of O1s peak, indicating that the BSB network produced at high-temperature pyrolysis had more oxygencontaining functional groups. The Van Krevelen plot (Fig. 1d) further demonstrates that high-temperature pyrolysis leads to stronger electron donor-acceptor interactions in the biochar due to a lower H/C ratio, which causes more efficient degradation of organic pollutants through intermolecular forces (e.g. electrostatic, charge transfer, and hydrophobic) [16]. Compared with the pristine raw seaweed, each BSB showed significantly improved aromaticity according to the elemental analysis. When the temperature was increased from 300 to 700 °C, the H/C atomic ratio decreased implying stronger degree of carbonization, which resulted in higher degree of aromaticity and hydrophobicity both facilitated PAH removal [28]. The high carbon and low oxygen content of BSB also increased its resistance against hydrolysis and chemical reactions, i.e., a chemically more stable product [36]. Pyrolysis at 700 °C led to an increase in carbon content from 31 wt% in raw seaweed to 34 wt%, which broadened the pyrolysis zone and promoted the formation and stability of BSB. Huang et al. (2020) reported that seaweed biochars prepared at pyrolysis temperature of 700 °C (BC700) exhibited higher aromatic and graphic structures than those prepared at  $\leq$  600 °C (BC600); subsequently BC700 better activated persulfate with the production of more reactive oxygen species (ROS) and enhanced the degradation of organic contaminants (e.g., PAHs) [37]. Moreover, we have observed recently that red algae biochars prepared at 900 °C exhibited remarkable 4-nonylphenol degradation capacity [13]. Therefore, the activation of PMS by BSB prepared at high pyrolysis temperature of 900 °C for the remediation of environmental matrices contaminated by recalcitrant PAHs need further evaluation. It has been reported that porosity or pore structure (e.g., pore size and distribution) is an important physicochemical property of biochars [38]. The results showed that pore size of BSB followed the order: BSB700 (8  $\mu m$ ) >BSB500 (6  $\mu$ m) > BSB300 (4  $\mu$ m) (Fig. 2a-c). BSB700 was more porous with extensively connected graphitized carbon network skeleton greater than BSB500 and BSB300. The porosity, namely, number of pore, increased gradually due to the chemical reactions between CaO/CaCO<sub>3</sub> and graphite-like phases of BSB. The high pyrolysis temperature could significantly govern the formation of graphitized carbon skeleton in biochars, which resulted in high surface functionality and porosity, and ultimately enhanced the catalytic degradation of contaminants during environmental remediation [13]. Besides, the pyrolysis temperatures at < 700 °C were suitable for the development of high-porosity structure</p> biochars [39]. It is also noteworthy that pyrolytic production of biochars at temperature of 600–700 °C leading to superior performance because high pyrolysis temperature altered the surface structure, the degree of carbonization, and the generation of specific surface area, which aided in sediment remediation [38]. Therefore, BSB700 was selected as the biochar catalyst for PAH degradation experiments.

#### 3.2. PAH degradation by PMS over BSB

The total PAH content (TPAH) in the untreated sediment was 60  $\pm$ 2.7 µg/dw-g. Among the 16 PAHs monitored, PH, BbF, FLU, BaA, and IP were the major species in the untreated sediment, with 4-ring PAHs (i.e., PH) being the major species (i.e., 36 % of TPAH). Generally, molecular weight and ring number govern the degradation efficiency of a PAH. TPAH collects many congeners having more than two aromatic rings. For simplicity sake, TPAH was classified as those of low molecular weight (LPAH: 2-3 rings, associated with industrial and domestic fuel combustion) and high molecular weight (HPAH: 4-6 rings, associated with combustion of fossil fuels and their products) [3]. Fig. 3a depicts the degradation of PAHs through SO<sub>4</sub>-mediated AOP in pure PMS and BSB/PMS treatment systems. The degradation of TPAH by PMS after 10 h was only 55 % due to weak oxidation ability of PMS. In the BSB/PMS system, the TPAH degradation was significantly improved to 77 % by PMS activation. Therefore, there was a synergistic effect between BSB and PMS on PAH degradation. The degradation of LPAHs and HPAHs by the BSB/PMS treatment was 79 and 75 %, respectively, which was higher than that of PMS-only process (73 and 40 %), individually). The degree of degradation of individual PAH species (by PMS and BSB/PMS) were 86 and 91 %, 72 and 91 %, 62 and 77 %, 26 and 46 %, and 48 and 89 %, for PH, BbF, FLU, BaA, and IP (Fig. 3b), respectively. Clearly, the performance of the BSB/PMS was significantly better than that of PMS in degrading all PAHs. With respect to ring number on PAH removal, the maximum removal was 87, 79, 67, 55, and 56 % for the 6-, 5-, 4-, 3-, and 2-ring PAHs, respectively (Fig. 3c). A possible explanation for results observed (ranking  $6 > 5 > 4 > 2 \approx 3$ -ring) is that BSB enhances the reversible donation and acceptance of electrons, due to its highly disordered amorphous structure containing abundant oxygen functionalities and the generation of  $SO_4^- \bullet$  with aromatic compounds on the BSB surface that resulted in higher degradation efficiency. The Ca<sup>2+</sup> species has been reported to exhibit excellent catalytic performance [40]. Ca<sup>2+</sup> ion, an electron-transfer mediator, generated SO4 • radical through electrophilic reactions with aromatic compounds to promote the PMS-based oxidation reaction. Moreover, after thermal conversion of seaweed into a carbon matrix, there were abundant free-flowing  $\pi$ -electrons enabling efficient electron transfer between the BSB surface and contaminant chemicals in question, and enabled PMS activation toward PAH degradation [26]. Previous studies have suggested that C=O is the active site for the catalytic decomposition of PMS because lone-pair electrons on C=O tend to bond with the O-O group of PMS, and facilitate single electron transfer to produce  $SO_4^{\bullet-}$  and  $HO_{\bullet-}$  bond during the reaction (Eqs. (1) and (2)) [30,41].

$$HSO_5^- + e^- \rightarrow SO_4^- \bullet + HO^- \tag{1}$$

$$HSO_5^- + e^- \rightarrow HO\bullet + SO_4^{2-}$$
 (2)

Therefore, one could conclude that the synergistic effect between  ${\rm HSO}_5^-$  and BSB resulted in high catalytic reactivity because of the production of radicals in the presence of PMS for PAHs degradation.

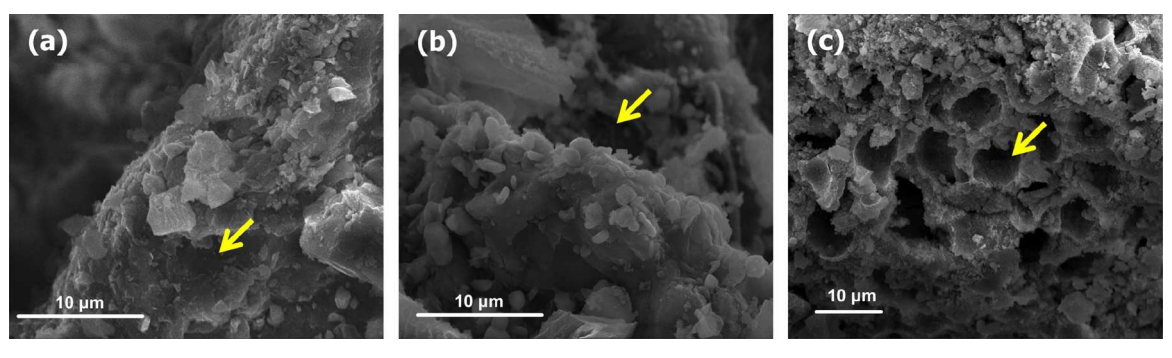


Fig. 2. The SEM images of (a) BSB300, (b) BSB500, and (c) BSB700 catalyst. The yellow arrow shows the correspondingly selected observation area.

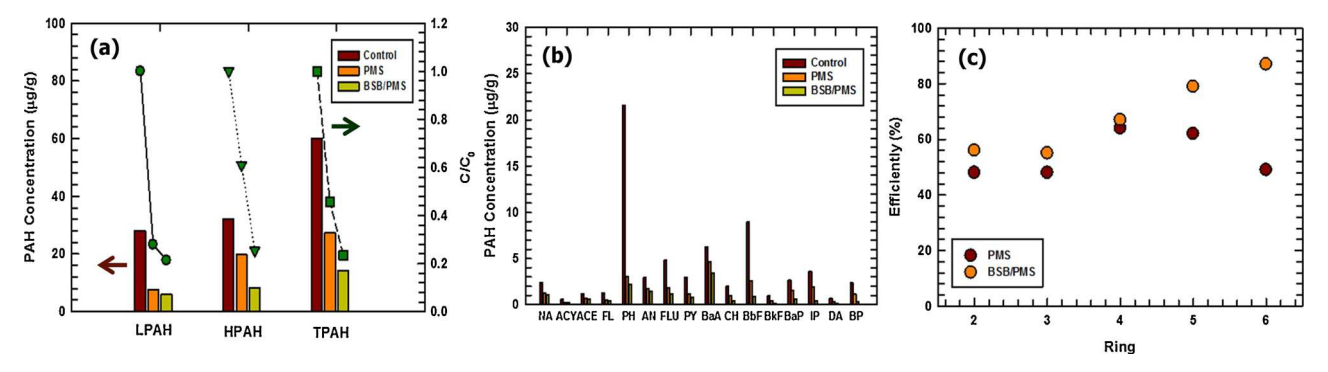


Fig. 3. The effectiveness of combined BSB and PMS treatment on the removal of LPAH, HPAH and TPAHs (a), individual PAH species (b), and percentage of PAH removal in terms of ring number (c) from aquatic sediments. Experimental conditions: sediment =1.00 g, reaction volume =40 mL, T =25 °C, pH<sub>0</sub> = 3.0, [PMS] = 1  $\times$  10<sup>-5</sup> M, [BSB] =3.0 g/L, molar ratio of PMS:  $\Sigma$ PAHs = 1:1.

Fig. 4a–c show the degradation of PAHs in the PMS system in terms of molecular weight of PAH (Fig. 4a), individual PAH (Fig. 4b) and ring number of PAH (Fig. 4c) as affected by the  $\Sigma$ [PAH]:[PMS] ratio. The TPAH degradation was 55, 40, and 10 % at  $\Sigma$ [PAH]:[PMS] of 1:1, 1:10, and 1:100, respectively. The TPAH degradation decreased markedly as the PMS dosage was increased from 0.01 to 1.0 mM (or increasing  $\Sigma$ [PAH]:[PMS] from 1:1 to 1:100) (Fig. 4a). Results agreed with what were reported by Wang and Wang (2020) demonstrated that SO4radical contributed to PAH degradation at high PMS concentrations [42]. However, further increase in PMS dosage to  $1 \times 10^{-4}$  and  $1 \times 10^{-3}$ M only yielded limited improvement in PAH degradation, which could be attributed to the scavenging of  $SO_4^{\bullet-}$  by excess PMS. Hence, 0.01 mM PMS (or  $\Sigma[PAH]$ :[PMS] = 1:1) was the optimal PMS dosage. Herein, four PAHs (ACY a LPAH; AN, BkF, and DA HPAHs) were observed in the treated sediments at relatively trace content, with PH (85 %), BbF (71 %), and FLU (61 %) exhibiting the highest extent of degradation (Fig. 4b). At the optimal PMS dosage of  $1 \times 10^{-5}$  M, the degradation of 6-, 5-, and 4-ring HPAHs was 49, 62, and 64 %, respectively, under otherwise identical experimental conditions (Fig. 4c).

The pyrolysis temperature is an important factor affecting the yield and catalytic property of biochar [43]. Fig. 5a shows that the TPAH degradation capacity increased significantly when the calcination temperature for BSB was increased from 300–700 °C. BSB700 exhibited catalytic degradation of LPAHs of 79 %, which was 55 % more than that of BSB300. Wang and Wang (2020) reported that biochar activated PMS via zigzag edges, defective structure, oxygen-containing surface functional groups, and electron transfer between the reactive species and pollutants in question [42]. Results clearly indicated that BSB enhanced the oxidative degradation of PAH by accelerating the decomposition of PMS to SO4 which facilitated charge transfer on BSB surface. The BSB700/PMS system exhibited the highest degradation efficiency of 91, 90, 89, 87, and 85 % for BbF, PH, IP, BP, and BkF, respectively (Fig. 5b).

Likewise, the degradation efficiency for the 6-, 5-, 4-, 3-, and 2-ring HPAHs were 87, 79, 67, 55, and 56 %, respectively (Fig. 5c). Therefore, 700 °C was selected as the best pyrolysis temperature for the preparation of BSB in subsequent experiments.

The influence of BSB concentration (1.0-7.0 g/L) on PAH removal was also studied at fixed PMS dosage of  $1\times 10^{-5}\, \mbox{M}$  and reaction time of 10 h. Fig. 6a gives the removal of TPAHs with respect to BSB dosage. It was clearly indicated that high BSB dosage improved the TPAHs degradation capacity, following the order: 7.0 g/L (88 %) > 3.0 g/L (77 %) > 1.0 g/L (35 %). More BSB in the system brought about more redox centers to activate the PMS, thereby enhancing the production of strong electron donors, specifically,  $SO_4^{\bullet-}$  and  $\bullet OH$ . Results agreed well with that reported recently by Luo et al. [44]. Furthermore, the degradation percentage of HPAH and LPAH were both increased from 11 to 88 % and 63–88%, respectively, when the BSB dosage was increased from 1.0–7.0 g/L, correspondingly. At the highest BSB concentration of 7.0 g/L, the degradation efficiency was 96, 95, 94, 93, and 92 % for BbF, IP, BP, DA, and BkF, individually (Fig. 6b), while that for the 6-, 5-, 4-, 3-, and 2-ring PAHs were 94, 89, 84, 67, and 72 %, respectively (Fig. 6c). Xiao et al. (2020) reported that the degradation efficiency was increased by increasing the BSB dosage due to subsequent increase in the production of SO<sub>4</sub>•- and •OH, which could trigger a series of chain reactions to accelerate PAH degradation [45]. Obviously, the biochar matrix generated abundant reactive oxygen species necessary for PAH degradation [46].

Fig. 7a gives results the removal of LPAH, HPAH and TPAH as a function of initial pH. The maximum TPAH degradation efficiency of 77 % occurred at the initial pH of 3.0 and decreased to 67 % at pH 9.0 because of elevated OH $^-$  reaction with SO<sub>4</sub>• $^-$  to yield HO• the latter was a weaker oxidant than the former [35]. The degradation efficiency declined from 79 to 68 % and 75 to 64 % for LPAHs and HPAHs, individually, when the pH was increased from 3.0–9.0. At pH 3.0, the

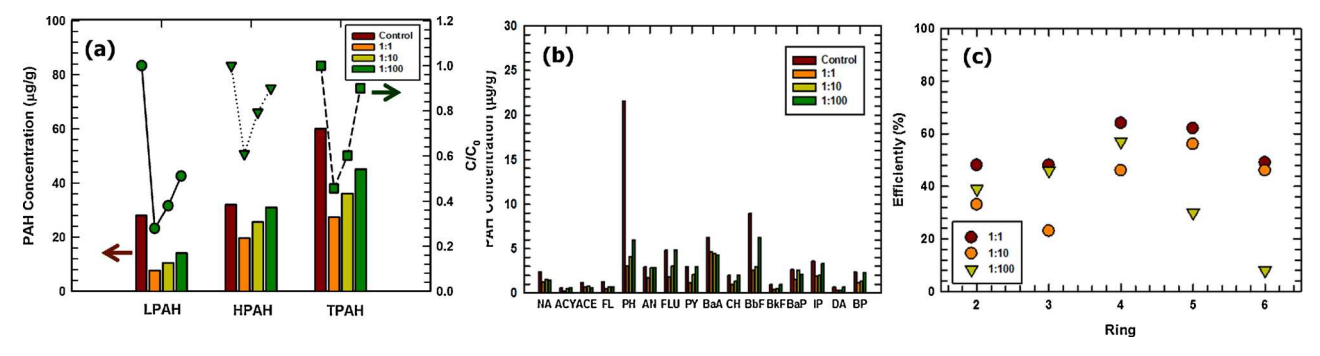


Fig. 4. The effect of PMS dosage (molar  $\Sigma$ [PAH]:[PMS] ratio) on the removal of LPAH, HPAH, and TPAHs (a), individual PAHs species (b), and percentage of PAH removal in terms of ring number (c) from aquatic sediments. Experimental conditions: [sediment] =1.00 g, reaction volume =40 mL, reaction time =10 h, T =25 °C, pH<sub>0</sub> = 3.0.

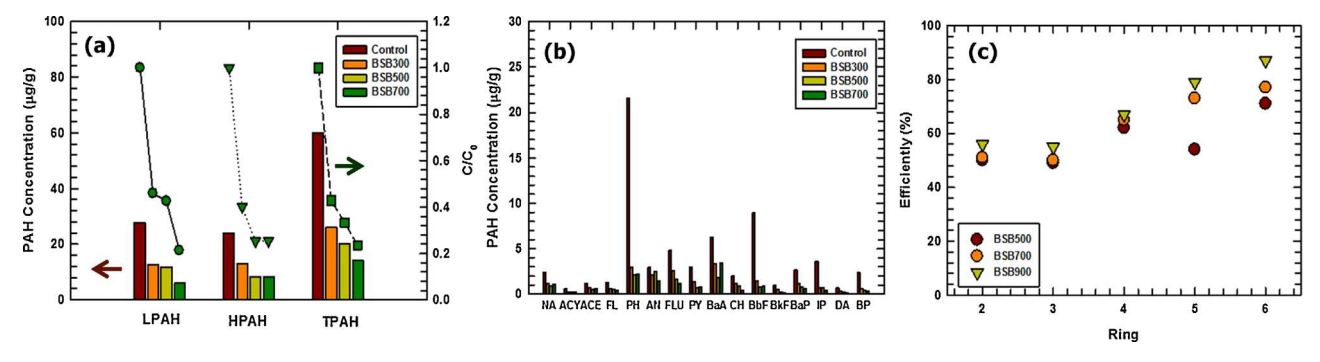


Fig. 5. The effect of pyrolysis temperature on the preparation of BSB biochar and its application for the degradation of LPAH, HPAH, and TPAH (a), individual PAH species (b), and percentage of PAH removal in terms of ring number (c) from aquatic sediments. Experimental conditions: [sediment] =1.00 g, reaction volume =40 mL, reaction time =10 h, T = 25 °C, D = 3.0, D

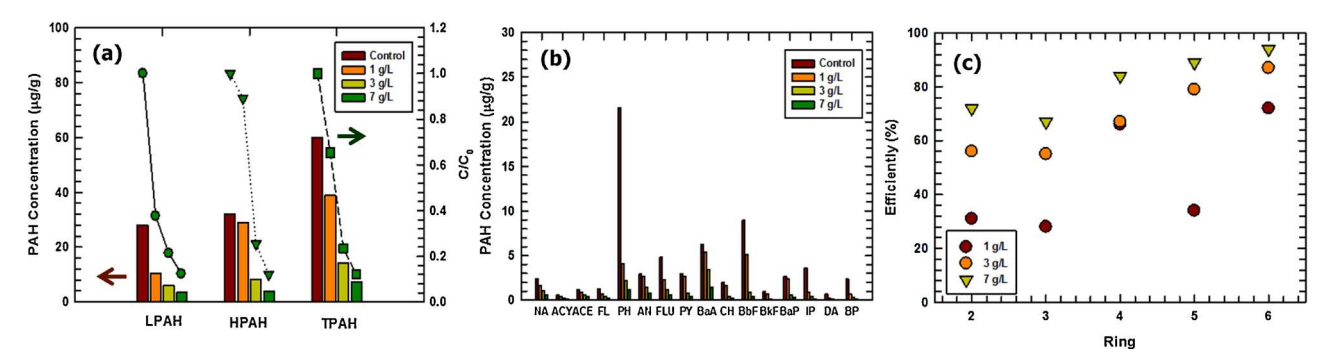


Fig. 6. The effect of BSB catalyst dosage on the degradation of LPAH, HPAH and total PAHs (a), individual PAH species (b), and percentage of PAH removal in terms of ring number (c) from aquatic sediments. Experimental conditions: [sediment] =1.00 g, reaction volume =40 mL, reaction time =10 h, T =25 °C, pH<sub>0</sub> = 3.0, [PMS] =  $1 \times 10^{-5}$  M, molar ratio of PMS:  $\Sigma$ PAHs = 1:1.

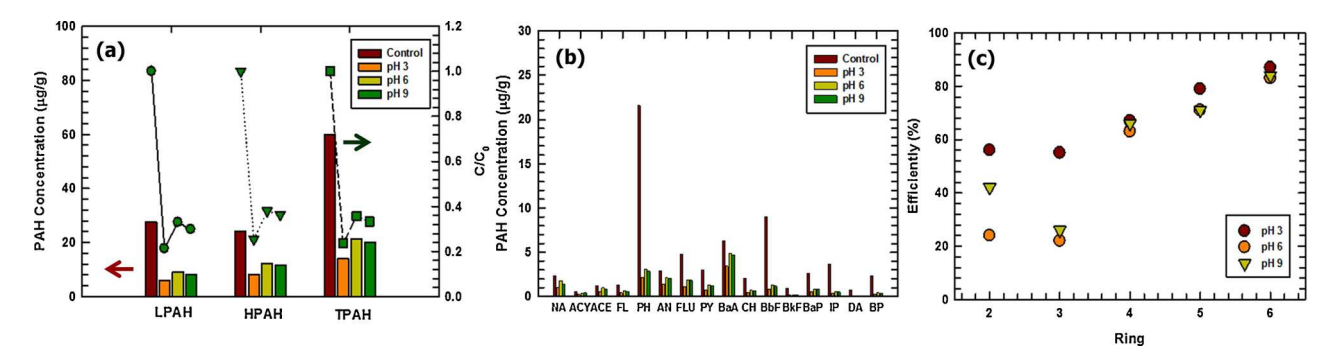


Fig. 7. The effect of initial pH on the degradation of LPAH, HPAH and TPAH (a), individual PAH species (b), and percentage of PAH removal in terms of ring number (c) from aquatic sediments. Experimental conditions: [sediment] =1.00 g, reaction volume =40 mL, reaction time =10 h, T =25 °C, [PMS] =  $1 \times 10^{-5}$  M, [BSB] =3.0 g/L, molar ratios of PMS:  $\Sigma$ PAHs = 1:1.

highest degradation was observed for IP, BbF, PH, ACY, and NA (Fig. 7b). The PAHs removal efficiency generally increased with ring number (Fig. 7c). The removal efficiency of 2- and 3- ring PAH at pH 6.0 and 9.0 was lower than that at pH 3.0. The average removal efficiency of HPAHs, i.e., 4-, 5- and 6-ring, was high, 78, 74, and 74 %, respectively, at pH 3.0, 6.0, and 9.0. The average removal efficiency of LPAHs, i.e., 2- and 3-ring was 56, 23, and 35 %, at pH 3.0, 6.0, and 9.0, respectively. The effect of initial pH on LPAHs degradation was more significant than that on HPAHs. The degradation of PAHs was mainly result of radical attack on the ring structure, i.e., hydrogen absorption of free radicals such as HO• and  $SO_4\bullet^-$ . HPAHs has more active hydrogen sites for radical absorption, therefore, the degradation of HPAHs was much enhanced than that of LPAHs. The relatively higher degradation efficiency of LPAHs at pH 3.0 than pH 6.0 and 9.0, could be attributed to the presence of radical scavengers, specifically, bicarbonate, at abundant

quantity in the pH range of 6.0–9.0. Alkalinity is commonly present in the aquatic systems, including sediments. LPAHs encountered double jeopardies, low hydrogen content and radical scavengers, especially at high pH. Overall, results indicated that the degradation of HPAHs was more complete than that of LPAHs at pH 3.0 over the reaction of 10 h, which was consistent with previous results [5]. Therefore, a low initial pH (3.0) is preferred because acid-catalysis in the PMS system facilitates the formation of  ${\rm SO_4}^{\bullet-}$  free radical. Both  ${\rm SO_4}^{\bullet-}$  and  ${\bullet}{\rm OH}$  radicals were equally responsible for PAHs degradation under acidic pH conditions. However, in the BSB/PMS process,  ${\rm SO_4}^{\bullet-}$  radical was the main active species generated from PMS rather than the  ${\bullet}{\rm OH}$  radicals. The pKa1 and pKa2 values of PMS are 0 and 9.4, respectively. Therefore, HSO5 was the dominant species of PMS at pH < 9.4 [4]. Indeed, our results indicated that the BSB/PMS process was intact and capable of carrying out PAH degradation over a wide range of pH. Consequently, control of the BSB

dose is option for minimizing the inhibitory effects of BSB toward  $SO_4^{\bullet-}/\bullet OH$  production. Meanwhile, alkaline pH condition decreased the oxidation potential of  $SO_4^{\bullet-}$  because  $OH^-$  scavenged  $SO_4^{\bullet-}$  concurrently at significant levels. Moreover, pH is a master variable affecting the uptake and subsequent catalysis degradation of PAHs over BSB. Overall, although pH significantly affected PAH degradation by the BSB/PMS process, the degradation efficiency remained effective over a wide pH range of 3.0–9.0.

It can be noted from Table 1 that the co-application of PDS, magnetic oxide, and biochars obtained by the pyrolysis of carbon - based feedstock such as bamboo [4], woody [5], and sludge [14], enhanced chemical oxidation efficiency in the treatment of PAH - contaminated sediments. Under optimum operation conditions, the PAHs degradation was 77 % under remediation time of 10 h, which was somewhat below that of other biochars, e.g., 86 % for  $Fe_3O_4-BB/PDS$  [4], 84 % for Fe<sub>3</sub>O<sub>4</sub>-WB/PDS [5], and 88 % for Fe/Mn - SBC/SPC (88 %) [14]. Results in Table 1 show that biochars modified with magnetic metallic (iron and manganese) exhibited superior (better degradation efficiency the 6-, 5-, 4-, 3-, and 2-ring PAHs) PAHs degradation due to synergistic action in ROS generation, electron transfer, adsorption, and catalytic capability, mainly at high catalyst dose of 3.3 g/L and an acidic pH (pH<sub>0</sub> = 3.0). The above results indicated that the addition of magnetic oxide-modified biochars was more effective in PAHs degradation than pristine biochars. Therefore, further investigation on the surface modification of engineered BSB and its effects on the degradation of PAHs in marine sediments is ongoing. Finally, the generation of reactive radical species due to BSB activation of PMS was verified by EPR analysis (Fig. 8). The EPR spectrum showed seven main peaks typical of 5, 5-dimethylpyrroline-(2)-oxyl-(1) (DMPOX) [35], indicating that SO<sub>4</sub>• was dominant in the degradation of PAHs. Meanwhile, since DMPO--HO•exhibited a smaller signal than that of DMPO-SO<sub>4</sub>•-, therefore BSB activation of PMS first formed  $SO_4^{\bullet-}$ , which was then converted to  $HO_{\bullet}$ by reaction with OH<sup>-</sup> under alkaline pH conditions. Based on the above results, it is possible to propose a mechanism for the activation of PMS on BSB toward PAH degradation in the complex sediment matrix. In most carbon-activated PMS processes, SO4 - and HO•were major reactive oxygen species responsible for the degradation of hazardous organic chemicals [19]. Therefore, both SO4 •- and HO• appeared in the BSB/PMS system, and SO4 - can be quickly converted into HO in aqueous solution via a nucleophilic substitution reaction. The addition of PMS to water released HO• and HSO<sub>4</sub> (Eqs. (3) and (4)), which were further decomposed to SO<sub>4</sub>•, HO• and weaker oxidants (SO<sub>5</sub>• and  $HO_{2}$  (Eqs. (5)–(10)) to trigger numeral synergistic reactions, e.g., charge transfer on BSB (Eqs. (11) and (12)). Consequently, SO<sub>4</sub>• and HO• were being continuously produced by a series of cyclic reactions to attack the PAHs and rendered them into smaller organic acids before being ultimately mineralized into CO<sub>2</sub> and H<sub>2</sub>O (Eq. (13)).

$$HSO_5^- + H_2O \rightarrow 2HO \bullet + H^+$$
 (3)

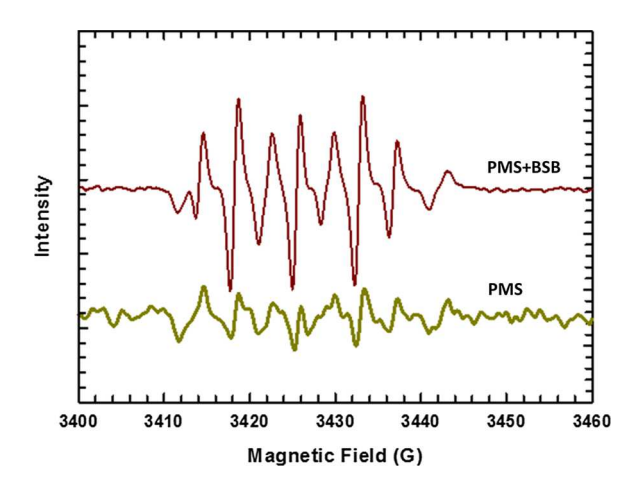


Fig. 8. Determination of reactive species by EPR in the BSB/PMS system.

$$HSO_5^- + H_2O \rightarrow H_2O_2 + HSO_4^-$$
 (4)

$$HSO_5^- \to SO_4 \bullet^- + HO \bullet \tag{5}$$

$$HSO_5^- + SO_4 \bullet^- \to SO_5 \bullet^- + SO_4^{2-} + H^+$$
 (6)

$$HSO_5^- + HO \bullet \rightarrow SO_5 \bullet^- + H_2O \tag{7}$$

$$HSO_5^- + HO \bullet \rightarrow HO_2 \bullet + SO_4^{2-} + H^+$$
(8)

$$SO_4 \bullet^- + H_2O \to SO_4^{2-} + HO \bullet + H^+$$
 (9)

$$SO_4 \bullet^- + OH^- \to SO_4^{2-} + HO \bullet \tag{10}$$

$$BSB + HSO_5^- \rightarrow BSB^+ + SO_4^- \bullet + HO^-$$
 (11)

$$BSB + HSO_5^- \rightarrow BSB^+ + HO \bullet + SO_4^{2-}$$
 (12)

$$PAHs + SO_4 \bullet^- + HO \bullet + O_2 \rightarrow byproducts + CO_2 + H_2O$$
 (13)

The process of BSB activation of PMS is complex, because of multiple radicals, namely, SO<sub>4</sub><sup>-</sup> and HO• present in the system and the addition of electrophilic SO<sub>4</sub><sup>-</sup> to aromatic rings being the major oxidation reaction (Fig. 9). It has been reported that calcium ion in biochar catalyst creates oxygen vacancy, i.e., O<sub>2</sub> adsorption site, and produces reactive oxygen on the calcium-based biochar surface [47]. In short, BSB activation of PMS produced SO4• and HO•. Calcium oxide and calcium carbonate on BSB surface promoted charge transfer between SO<sub>4</sub>• radical and PAHs, then further electron transfer activated PMS to produce HO•radical. Notwithstanding that BSB/PMS treatment achieved significant elimination of PAHs from contaminated sediments, further studies are necessary to determine the degree of CO<sub>2</sub> conversion in the remediation of PAH-contaminated marine sediments by the BSB/PMS

Sulfate/hydroxyl radical based AOPs using biochar — based catalysts originated from various feedstocks for the degradation of PAH — contaminated sediments.

				•	•	
Feedstock	Catalyst	Pyrolysis temperature (°C)	Oxidant	Optimum operating conditions	Maximum degradation rates	Refs.
Bamboo	Fe <sub>3</sub> O <sub>4</sub> -BB	300	PDS	$pH_0=3.0, [Fe_3O_4-BB]=3.3 \text{ g/L}, [PDS]: \sum \\ [PAH]=1:1, \text{ and 24 h reaction time}$	86 % PAHs elimination; maximum degradation of 99, 88, 86, 81, and 79% for the 6-, 5-, 4-, 3-, and 2-ring PAHs	[4]
Woody	Fe <sub>3</sub> O <sub>4</sub> -WB	300	PDS	$pH_0=3.0, \ [Fe_3O_4-WB]=3.3 \ g/L, \\ [PDS]: \sum [PAH]=1:1, \ and \ 24 \ h \ reaction \\ time$	84 % PAHs degradation; maximum degradation of 90, 84, 87, 80, and 64% for the 6-, 5-, 4-, 3-, and 2-ring PAHs	[5]
Fe/Mn-rich sludge	Fe/Mn – SBC	700	SPC	$pH_0=11.0, \ [Fe/Mn-SBC]=1.7 \ g/L, \\ [SPC]: \sum [PAH]=10:1, \ and \ 6 \ h \ reaction \\ time$	88 % PAHs elimination; maximum degradation of 90, 85, 83, 70, and 42% for the 6-, 5-, 4-, 3-, and 2-ring PAHs	[14]
Brown seaweed	BSB	700	PMS	$pH_0 = 3.0, \mbox{[BSB]} = 3.0 \mbox{ g/L}, \mbox{[PMS]:} \sum \mbox{[PAH]} = 1.1, \mbox{ and } 10 \mbox{ h reaction time}$	77 % PAHs removal; maximum degradation of 87, 79, 67, 55, and 56% for the 6-, 5-, 4-, 3-, and 2-ring PAHs	This study

SPC: sodium percarbonate; PDS: peroxydisulfate; PMS: peroxymonosulfate; PAH: polycyclic aromatic hydrocarbons; BB: bamboo biochar; WB: woody biochar; SBC: sludge biochar; BSB: brown seaweed biochar.

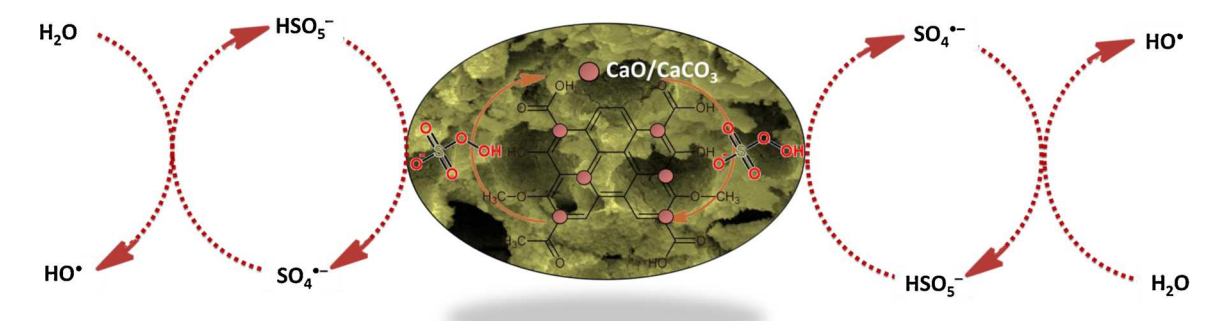


Fig. 9. Proposed degradation mechanism of PAH over BSB catalyst in the sulfate and hydroxyl radical-based advanced oxidation processes.

system. It is expected that complex matrixes of the marine environment will affect the mineralization of PAHs in the BSB/PMS remediation process.

#### 4. Conclusion

A brown seaweed was pyrolyzed at temperature in the range of 300 and 700 °C to synthesize brown seaweed biochar (BSB). The biochar synthesized at 700 °C in  $CO_2$  atmosphere, i.e., BSB700, was highly thermal stable and effectively degraded PAHs from contaminated aquatic sediments in acidic media. BSB700 exhibited high capacity in activating PMS to produce  $SO_4\bullet^-$  and  $HO\bullet$  radicals. Results showed that PAHs with two to six benzene rings were readily degraded over a wide range of pH (3.0–9.0) in the BSB matrix. Overall, the proposed technology uses seaweed, a renewable biomass feedstock, to make biochar for application in the BSB/PMS system that exhibited excellent capability in removing environmental contaminants such as PAHs from contaminated sediments. Overall, results clearly demonstrated the potentials of using aquatic biomass for environmental remediation applications.

### CRediT authorship contribution statement

Chang-Mao Hung: Conceptualization, Methodology, Investigation, Validation, Formal analysis, Writing - original draft. Chin-Pao Huang: Writing - review & editing, Visualization. Jia-Wei Cheng: Formal analysis. Chiu-Wen Chen: Resources. Cheng-Di Dong: Resources, Supervision.

#### **Declaration of Competing Interest**

The authors report no declarations of interest.

#### Acknowledgments

The authors would like to thank the Ministry of Science and Technology of Taiwan for financial support of this study under Contract No. 108-2221-E-992-051-MY3. Addition support was provided by US NSF IOA grant No. 1632899 (to CPH).

# References

- [1] J. Jang, V.E. Forbes, M.J. Sadowsky, Lack of evidence for the role of gut microbiota in PAH biodegradation by the polychaete *Capitella teleta*, Sci. Total Environ. 725 (2000), 138356.
- [2] L. Li, C. Lai, F. Huang, M. Cheng, G. Zeng, D. Huang, B. Li, S. Liu, M. Zhang, L. Qin, M. Li, J. He, Y. Zhang, L. Chen, Degradation of naphthalene with magnetic bio-char activate hydrogen peroxide: synergism of bio-char and Fe–Mn binary oxides, Water Res. 160 (2019) 238–248.
- [3] S.P. Maletić, J.M. Beljin, S.D. Rončević, M.G. Grgić, B.D. Dalmacija, State of the art and future challenges for polycyclic aromatic hydrocarbons is sediments: sources, fate, bioavailability and remediation techniques, J. Hazard. Mater. 365 (2019) 467–482.

- [4] C.D. Dong, C.W. Chen, C.M. Hung, Synthesis of magnetic biochar from bamboo biomass to activate persulfate for the removal of polycyclic aromatic hydrocarbons in marine sediments, Bioresour. Technol. 245 (2017) 188–195.
- [5] C.D. Dong, C.W. Chen, C.M. Kao, C.C. Chien, C.M. Hung, Wood-biochar-supported magnetite nanoparticles for remediation of PAH-contaminated estuary sediment, Catalysts 8 (2018) 73–86.
- [6] C.D. Dong, M.L. Tsai, C.W. Chen, C.M. Hung, Remediation and cytotoxicity study of polycyclic aromatic hydrocarbon-contaminated marine sediments using synthesized iron oxide-carbon composite, Environ. Sci. Pollut. Res. 6 (2018) 5242, 5252
- [7] C.D. Dong, C.W. Chen, M.L. Tsai, J.H. Chang, S.Y. Lyu, C.M. Hung, Degradation of 4-nonylphenol in marine sediments by persulfate over magnetically modified biochars, Bioresour. Technol. 281 (2019) 143–148.
- [8] C.D. Dong, C.P. Huang, T.B. Nguyen, C.F. Hsiung, C.H. Wu, Y.L. Lin, C.W. Chen, C. M. Hung, The degradation of phthalate esters in marine sediments by persulfate over iron–cerium oxide catalyst, Sci. Total Environ. 696 (2019) 133973–133982.
- [9] C.D. Dong, Y.C. Lu, J.H. Chang, T.H. Wang, C.W. Chen, C.M. Hung, Enhanced persulfate degradation of PAH-contaminated sediments using magnetic carbon microspheres as the catalyst substrate, Process Safety Environ. Prot. 125 (2019) 219–227.
- [10] C.D. Dong, C.W. Chen, M.L. Tsai, C.M. Hung, The efficacy and cytotoxicity of iron oxide-carbon black composites for liquid-phase toluene oxidation by persulfate, Environ. Sci. Pollut. Res. 26 (2019) 14786–14796.
- [11] C.D. Dong, C.W. Chen, T.B. Nguyen, C.P. Huang, C.M. Hung, Degradation of phthalate esters in marine sediments by persulfate over Fe–Ce/biochar composites, Chem. Eng. J. 384 (2020), 123301.
- [12] C.D. Dong, M.L. Tsai, T.H. Wang, J.H. Chang, C.W. Chen, C.M. Hung, Removal of polycyclic aromatic hydrocarbon (PAH)-contaminated sediments by persulfate oxidation and determination of degradation product cytotoxicity based on HepG2 and ZF4 cell lines, Environ. Sci. Pollut. Res. 27 (2020) 34596–34605.
- [13] C.M. Hung, C.P. Huang, S.L. Hsieh, M.L. Tsai, C.W. Chen, C.D. Dong, Biochar derived from red algae for efficient remediation of 4-nonylphenol from marine sediments, Chemosphere 254 (2020), 126919.
- [14] C.M. Hung, C.P. Huang, C.W. Chen, C.H. Wu, Y.L. Lin, C.D. Dong, Activation of percarbonate by water treatment sludge-derived biochar for the remediation of PAH-contaminated sediments, Environ. Pollut. 265 (2020), 114914.
- [15] C.M. Hung, C.P. Huang, S.S. Lam, C.W. Chen, C.D. Dong, The removal of polycyclic aromatic hydrocarbons (PAHs) from marine sediments using persulfate over a nano-sized iron composite of magnetite and carbon black activator, J. Environ. Chem. Eng. 8 (2020), 104440.
- [16] C.M. Hung, C.P. Huang, C.W. Chen, S.L. Hsieh, C.D. Dong, Effects of biochar on catalysis treatment of 4-nonylphenol in estuarine sediment and associated microbial community structure, Environ. Pollut. 268 (2021), 115673.
- [17] C.M. Hung, C.W. Chen, Y.J. Jhuang, C.D. Dong, Fe<sub>3</sub>O<sub>4</sub> magnetic nanoparticles: characterization and performance exemplified by the degradation of methylene blue in the presence of persulfate, J. Adv. Oxid. Technol. 19 (2016) 43–51.
- [18] C.M. Hung, C.W. Chen, Y.Y. Liu, C.D. Dong, Decolorization of methylene blue by persulfate activated with FeO magnetic particles, Water Environ. Res. 88 (2016) 675–686.
- [19] R.D.C. Soltani, M. Mahmoudi, G. Boczkaj, A. Khataee, Activation of peroxymonosulfate using carbon black nano-spheres/calcium alginate hydrogel matrix for degradation of acetaminophen: Fe<sub>3</sub>O<sub>4</sub> co-immobilization and microbial community response, J. Ind. Eng. Chem. 91 (2020) 240–251.
- [20] S. Giannakis, K.Y. Lin, F. Ghanbari, A review of the recent advances on the treatment of industrial wastewaters by sulfate radical-based advanced oxidation processes (SR-AOPs), Chem. Eng. J. 406 (2021), 127083.
- [21] S. Ye, G. Zeng, X. Tan, H. Wu, J. Liang, B. Song, N. Tang, P. Zhang, Y. Yang, Q. Chen, X. Li, Nitrogen-doped biochar fiber with graphitization from *Boehmeria nivea* for promoted peroxymonosulfate activation and non-radical degradation pathways with enhancing electron transfer, Appl. Catal. B Environ. 269 (2020), 118850.
- [22] W.A. Wan Mahari, W.L. Nam, C. Sonne, W. Peng, X.Y. Phang, R.K. Liew, P.N. Y. Yek, X.Y. Lee, O.W. Wen, P.L. Show, W.H. Chen, J.S. Chang, S.S. Lam, Applying microwave vacuum pyrolysis to design moisture retention and Ph neutralizing palm kernel shell biochar for mushroom production, Bioresour. Technol. 312 (2020), 123572.

- [23] T. Ren, N. Chen, W.A. Wan Mahari, C. Xu, H. Feng, X. Ji, Q. Yin, P. Chen, S. Zhu, H. Liu, G. Liu, L. Li, S.S. Lam, Biochar for cadmium pollution mitigation and stress resistance in tobacco growth, Environ. Res. 192 (2021), 110273.
- [24] Y. Yang, S. Ye, C. Zhang, G. Zheng, X. Tan, B. Song, B. Zhang, H. Yang, M. Li, Q. Chen, Application of biochar for the remediation of polluted sediments, J. Hazard. Mater. 404 (2021), 124052.
- [25] X. Zhao, Q.D. An, Z.Y. Xiao, S.R. Zhai, Z. Shi, Seaweed-derived multifunctional nitrogen/cobalt-codoped carbonaceous beads for relatively high-efficient peroxymonosulfate activation for organic pollutants degradation, Chem. Eng. J. 353 (2018) 7467–7596.
- [26] Y. Xie, W. Hu, X. Wang, W. Tong, P. Li, H. Zhou, Y. Wang, Y. Zhang, Molten salt induced nitrogen-doped biochar nanosheets as highly efficient peroxymonosulfate catalyst for organic pollutant degradation, Environ. Pollut. 260 (2020), 114053.
- [27] M.T. Yang, Y. Du, W.C. Tong, A.C.K. Yip, K.Y. Lin, Cobalt-impregnated biochar produced from CO<sub>2</sub>-mediated pyrolysis of Co/lignin as an enhanced catalyst for activating peroxymonosulfate to degrade acetaminophen, Chemosphere 226 (2019) 924–933.
- [28] J. Guo, X. Wen, J. Yang, Y. Fan, Removal of benzo(a)pyrene in polluted aqueous solution and soil using persulfate activated by corn straw biochar, J. Environ. Manage. 272 (2020), 111058.
- [29] F. Li, J. Chen, X. Hu, F. He, E. Bean, D.C.W. Tsang, Y.S. Ok, B. Gao, Applications of carbonaceous adsorbents in the remediation of polycyclic aromatic hydrocarboncontaminated sediments: a review, J. Clean. Prod. 255 (2020), 120263.
- [30] D. Ding, S. Yang, X. Qian, L. Chen, T. Cai, Nitrogen-doping positively whilst sulfur-doping negatively affect the catalytic activity of biochar for the degradation of organic contaminant, Appl. Catal. B Environ. 263 (2020), 118348.
- [31] X. Song, K. Li, P. Ning, C. Wang, X. Sun, L. Tang, H. Ruan, S. Han, Surface characterization studies of walnut-shell biochar catalysts for simultaneously removing of organic sulfur from yellow phosphorus tail gas, Appl. Surf. Sci. 425 (2017) 130–140.
- [32] E.E. Chang, C.H. Chen, Y.H. Chen, S.Y. Pan, P.C. Chiang, Performance evaluation for carbonation of steel-making slags in a slurry reactor, J. Hazard. Mater. 186 (2011) 558–564.
- [33] R.Z. Wang, D.L. Huang, Y.G. Liu, C. Zhang, C. Lai, X. Wang, G.M. Zeng, X.M. Gong, A. Duan, Q. Zhang, P. Xu, Recent advances in biochar-based catalysts: properties, applications and mechanisms for pollution remediation, Chem. Eng. J. 371 (2019) 380–403.
- [34] Z. Jia, Z. Gao, K. Kou, A. Feng, C. Zhang, B. Xu, G. Wu, Facile synthesis of hierarchical a-site cation deficiency perovskite La<sub>x</sub>FeO<sub>3-y</sub>/RGO for high efficiency microwave absorption, Compos. Commun. 20 (2020), 100344.

- [35] Y. Li, S. Ma, S. Xu, H. Fu, Z. Li, K. Li, K. Sheng, J. Du, X. Lu, X. Li, S. Liu, Novel magnetic biochar as an activator for peroxymonosulfate to degrade bisphenol A: emphasizing the synergistic effect between graphitized structure and CoFe<sub>2</sub>O<sub>4</sub>, Chem. Eng. J. 387 (2020), 124094.
- [36] S.S. Lam, R.K. Liew, Y.M. Wong, E. Azwar, A. Jusoh, R. Wahi, Activated carbon for catalyst support from microwave pyrolysis of orange peel, Waste Biomass Valorization 8 (2017) 2109–2119.
- [37] Y. Huang, X. Guo, Z. Ding, Y. Chen, X. Hu, Environmentally persistent free radicals in biochar derived from *Laminaria japonica* grown in different habitats, J. Anal. Appl. Pyrolysis 151 (2020), 104941.
- [38] Y. Yang, S. Ye, C. Zhang, G. Zeng, X. Tan, B. Song, P. Zhang, H. Yang, M. Li, Q. Chen, Application of biochar for the remediation of polluted sediments, J. Hazard, Mater. 404 (2021), 124052.
- [39] L. Leng, Q. Xiong, L. Yang, H. Li, Y. Zhou, W. Zhang, S. Jiang, H. Li, H. Huang, An overview on engineering the surface area and porosity of biochar, Sci. Total Environ. 763 (2021), 144204.
- [40] C. Li, M. Li, X. Bo, L. Yang, A.C. Mtukula, L. Guo, Facile synthesis of electrospinning Mn<sub>2</sub>O<sub>3</sub>-Fe<sub>2</sub>O<sub>3</sub> loaded carbon fibers for electrocatalysis of hydrogen peroxide reduction and hydrazineoxidation, Electrochim. Acta 211 (2016) 255–264.
- [41] M.M. Mian, G. Liu, H. Zhou, Preparation of N-doped biochar from sewage sludge and melamine for peroxymonosulfate activation: N-functionality and catalytic mechanisms, Sci. Total Environ. 744 (2020), 140862.
- [42] S. Wang, J. Wang, Kinetics of PMS activation by graphene oxide and biochar, Chemosphere 239 (2020), 124812.
- [43] T.D. Minh, J. Song, A. Deb, L. Cha, V. Srivastava, M. Sillanpää, Biochar based catalysts for the abatement of emerging pollutants: a review, Chem. Eng. J. 394 (2020), 124856.
- [44] J. Luo, S. Bo, Y. Qin, Q. An, Z. Xiao, S. Zhai, Transforming goat manure into surface-loaded cobalt/biochar as PMS activator for highly efficient ciprofloxacin degradation, Chem. Eng. J. 395 (2020), 125063.
- [45] S. Xiao, M. Cheng, H. Zhong, Z. Liu, Y. Liu, X. Yang, Q. Liang, Iron-mediated activation of persulfate and peroxymonosulfate homogeneous and heterogeneous ways: a review, Chem. Eng. J. 384 (2020), 123265.
- [46] A. Kumar, G. Sharma, M. Naushad, A.H. Al-Muhtaseb, A. García-Peñas, G.T. Mola, C. Si, F.J. Stadler, Bio-inspired and biomaterials-based hybrid photocatalysts for environmental detoxification: a review, Chem. Eng. J. 382 (2020), 122937.
- [47] H. Guo, X. Kou, Y. Zhao, S. Wang, Q. Sun, X. Ma, Effect of synergistic interaction between Ce and Mn on the CO<sub>2</sub> capture of calcium-based sorbent: textural properties, electron donation, and oxygen vacancy, Chem. Eng. J. 309 (2018) 22–29